

Seeded Supercontinuum Generation with Optical Parametric Down-Conversion

D. R. Solli,^{1,2} B. Jalali,¹ and C. Ropers²

¹*Department of Electrical Engineering, University of California, Los Angeles, Los Angeles, California 90095, USA*

²*Courant Research Center Nano-Spectroscopy and X-Ray Imaging, University of Göttingen, Göttingen, Germany*

(Received 18 August 2010; published 29 November 2010)

The transition between modulation instability gain and induced soliton fission in nonlinear fiber is experimentally investigated by coherent seeding with the two-color output of an optical parametric oscillator. This approach produces supercontinuum spectra displaying persistent, fine modulation from seeding-induced noise reduction. Numerical simulations support the findings.

DOI: [10.1103/PhysRevLett.105.233902](https://doi.org/10.1103/PhysRevLett.105.233902)

PACS numbers: 42.65.Re, 42.65.Sf, 42.81.Dp

Supercontinuum (SC) radiation, white light generated by spectral broadening in a nonlinear medium, has enhanced techniques and enabled revolutionary measurements in frequency metrology, ultrafast science, imaging, flow cytometry, communications, and other areas [1–5]. The generation of this white light has also been widely studied as a complex process presenting a variety of experimental and theoretical challenges [6]. Despite its widespread successes, SC stability remains a critical issue in many applications, and reduction of SC noise has the potential to improve measurement speed, sensitivity, and precision. Because of the long interaction lengths in optical fiber, large broadening factors can be obtained with relatively modest input power levels, particularly in the zero or anomalous dispersion regimes where multiple effects contribute. In general, however, there is a trade-off between the broadening factor and the spectral-temporal stability of the SC, owing to the role of noise in the nonlinear mechanisms [7–10].

Fluctuations are particularly pronounced for SC generated by comparatively long (e.g., picosecond or nanosecond) pulses, the form produced by many fiber lasers and other compact, turn-key sources. In this regime, a cascade process beginning with modulation instability (MI) followed by soliton fission and Raman scattering is triggered by noise, resulting in unstable spectral broadening. In extreme form, this process produces non-Gaussian (heavy-tailed) statistics and rare events known as optical rogue waves [11]. Nonetheless, for practical reasons, long-pulse-pumped SC sources are today the most commonly used form in life science applications, such as fluorescence nanoscopy [4]. Some of these disadvantages could be alleviated by a more widespread use of femtosecond SC; however, in many circumstances, including broadband coherent anti-Stokes Raman scattering (CARS) spectroscopy, modelocked narrowband pulses and broadband SC are simultaneously desired [12]. In applications such as fluorescence nanoscopy, long pulses are also needed [4].

Fibers with tailored dispersive and nonlinear properties have been used to produce SC in the long-pulse regime with increased stability [8,13–15]. Induced MI, which has been employed for a variety of purposes [16], has also been

suggested as a means of actively manipulating SC characteristics [7]. Recently, seeding was used to achieve a picosecond SC source with pulse-to-pulse coherence in uniform nonlinear fiber [17]. Other works have also considered the effect of added input modulation [18–20] and feedback [21] on SC generation.

Here, we map the spectral characteristics of MI gain and MI-induced soliton fission in a two-pulse (pump-seed) experiment. A scan of the relative pump-seed delay clearly resolves the continuous transition between these nonlinear processes. Excellent reproducibility and stability of the seeded SC is achieved by deriving the modelocked pump and seed waves for the first time from parametric down-conversion. The measurements, which are modeled within the generalized nonlinear Schrödinger equation, characterize the seeding and present a route towards practical implementation of active stimulation for low-noise, coherent SC generation with long pulses.

MI, a four-wave mixing process, creates spectral sidebands around a narrowband pump [16]; in the time domain, the pulse develops a growing amplitude modulation, leading to the formation of soliton precursors. As their amplitudes grow, one or more solitons are eventually ejected from the pulse (soliton fission [22]), undergoing a progressive redshift due to self-induced Raman scattering [7]. The process is either noise induced (occurring spontaneously) or can be actively stimulated. The challenge of coherent stimulation arises in generating a seed that is substantially wavelength-shifted from and modelocked to the pump. Standard electro- and acousto-optical modulators do not produce large enough shifts. Some optical processes such as Raman scattering can produce large shifts but must also be coherently seeded to produce a coherent output. In a previous experiment, coherent seeding was accomplished with a pulse derived from the pump itself: a portion of the pump was coherently broadened to some extent in a dispersion-managed fiber, and a seed pulse was carved from the spectral tail [17]. In that approach, the seed power level is low and its stability can become a limiting factor.

The method employed in the present work has distinct advantages in that it utilizes an optical parametric

oscillator (OPO) configured to produce strong, mode-locked signal and idler pulses at the proper wavelengths to pump and seed spectral broadening. Figure 1(a) shows the experimental setup used to produce a stimulated SC with an OPO. A titanium:sapphire laser at 795 nm pumps an OPO (80 MHz rep. rate) to produce signal and idler pulses at 1550 nm and 1633 nm. These pulses are coupled to fiber and separated with a filter. The 1550 nm pulses, which serve as the SC pump, are reduced to a 1 nm bandwidth and amplified with an erbium-doped fiber amplifier. The SC seed pulses at 1633 nm pass through a variable delay segment and are combined with the pump pulses for delivery to 15 m of highly nonlinear fiber (HNLF, dispersion: $\beta_2 = 1.13 \times 10^{-4} \text{ ps}^2/\text{nm}$, $\beta_3 = 6.48 \times 10^{-5} \text{ ps}^3/\text{nm}$, nonlinear coefficient: $\gamma = 10.66 \text{ W}^{-1} \text{ km}^{-1}$). By adding substantial dispersion to the seed prior to the HNLF, scanning the delay variable translates into varying the instantaneous seed wavelength; spectral and temporal resolutions are experimentally seen to be less than $\sim 2 \text{ nm}$ and 2 ps, respectively, limited by factors such as pump-seed walk-off and pump bandwidth. The light output from the HNLF is coupled either to an optical spectrum analyzer (OSA) for measurements of the optical spectrum or, after band pass filtering, to a photodetector

and radio-frequency (RF) spectrum analyzer for stability measurements [10].

The color-coded image in Fig. 1(b) displays the measured spectral output of the nonlinear mixing process as a function of seed time delay τ (relative to pump). Sections at constant delay and wavelength are displayed in Figs. 1(c) and 1(d), respectively. In Fig. 1(b), the main vertical stripes correspond to the pump (1550 nm, broadened by self-phase modulation) and the seed, which displays both a narrowband component (1633 nm) and a weak broader pedestal. In addition, strong diagonal components appear flanking the pump spectrum. Substantial spectral broadening is observed around the time delay ($\tau \sim 0$) where the main redshifted diagonal component intersects the vertical seed stripe [cf. Fig. 1(c)]. Fine spectral and temporal modulations that were stable throughout the measurement are observed across the image. The features in the image represent different aspects of MI and MI-induced soliton fission, as explained below.

The diagonal stripes further from zero delay arise from MI gain acting on the weak pedestal in the seed, which, due to the four-wave mixing nature of the process, appear symmetrically around the pump wavelength. The slopes

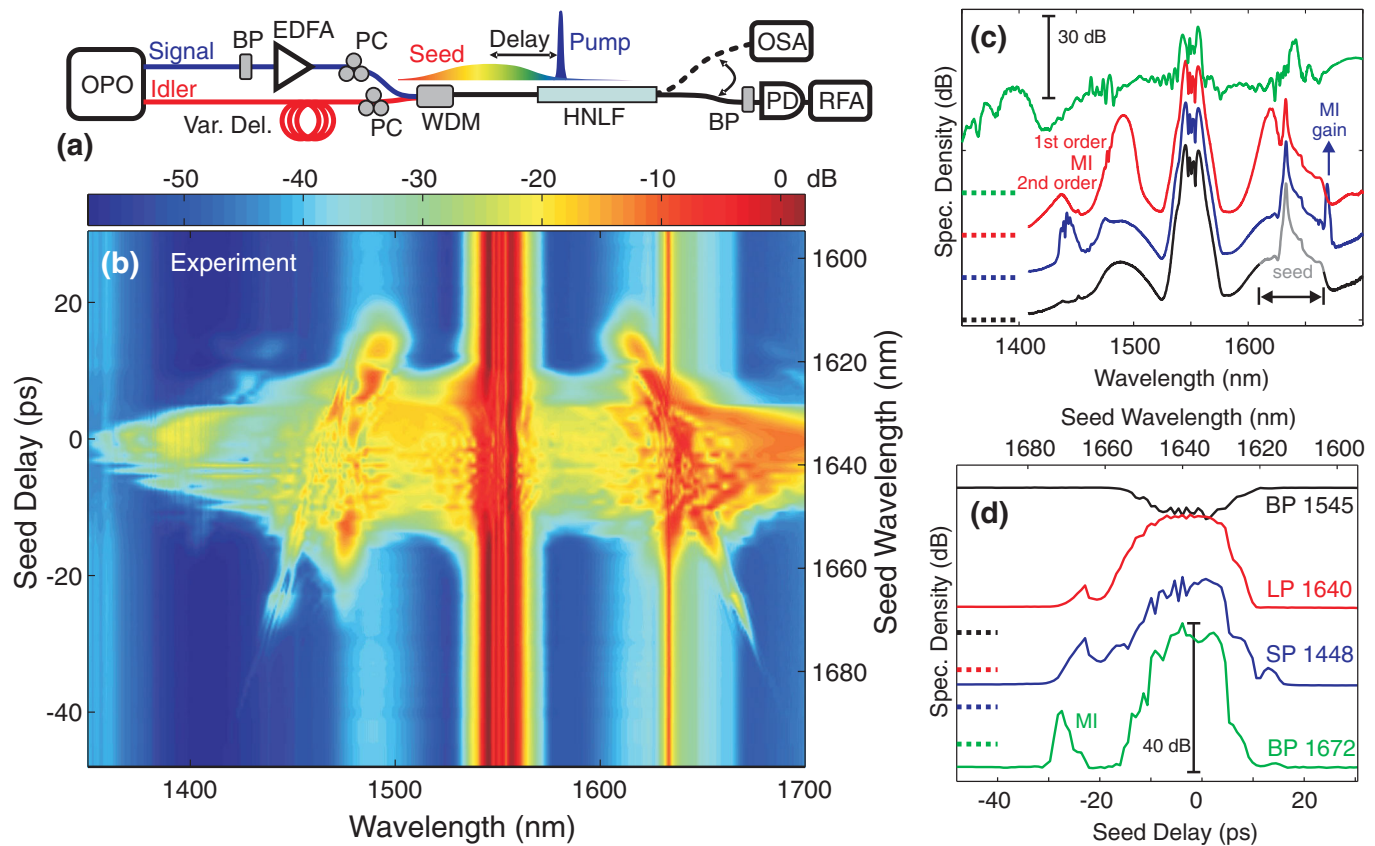


FIG. 1 (color online). (a) Experimental setup. (b) Output spectral density (color scale, dB) from the HNLF as a function of seed delay (avg. pump power $\sim 14 \text{ mW}$). (c) Spectral density vs wavelength (horizontal sections from b) at seed delays of (bottom to top) -48 ps , -26 ps , 12 ps , and -1 ps (note fine structure). Curves offset by 15 dB, dashed lines at -60 dB levels. Seed spectrum (gray, bottom trace) is superimposed on noise-induced MI lobe. (d) Spectral density vs seed delay at different spectral regions (vertical sections from b). By wavelength: BP 1545 (band pass, $\Delta\lambda \sim 3 \text{ nm}$), LP 1640 (long pass), SP 1448 (short pass), BP 1672 ($\Delta\lambda \sim 1 \text{ nm}$).

of these diagonals correspond to an anomalous group delay dispersion of ~ 0.8 ps/nm (intentionally applied as described above) experienced by the seed before entering the HNLF. The fact that this amplified MI signal is significantly narrower than the bandwidth of the spontaneous (noise-induced) MI lobes around the pump [cf. red (medium gray) curve in Fig. 1(c)] indicates that, for every delay, only a small spectral fraction of the seed is overlapping with the pump pulse. For this reason, these experiments can be interpreted in terms of quasi-continuous-wave (cw) stimulation. When sufficient seed intensity temporally and spectrally overlaps with the peak of the MI gain, soliton fission is initiated.

On the right of Fig. 1(b), a second axis gives the effective seed wavelength at each delay, which corresponds to the spectral component of the seed overlapping the pump pulse. The spectral seeding range (over which substantial broadening is produced) is substantially larger than the narrow portion of the seed spectrum [FWHM ~ 20 nm vs 1.6 nm, cf. Figs. 1(c) and 1(d)]. This indicates that even the weak seed pedestal is amplified enough by MI to result in soliton fission. Close to the transition, the MI amplitude is comparable to that of the narrowband seed component, which requires less MI amplification to begin soliton fission. The efficiency of the seeding is shown by the substantial pump depletion near zero delay [cf. Fig. 1(d)].

In order to model the features described, we simulate the pulse propagation with the generalized nonlinear Schrödinger equation (NLSE) [16,23]. Experimental pulse parameters are utilized, including power levels, pulse spectra, and dispersion. Figure 2(a) displays the simulated output spectra in the same manner as in Fig. 1(b). Good agreement between simulation and experiment is obtained, including the overall appearance and many specific spectral and temporal details, such as the transition from pure MI gain to soliton fission. Another feature common to both the experiment and simulation are weak secondary MI lobes visible on the blue and (partially) on the red sides of the spectrum. While it is not expected that specific fine details will be reproduced, the general distribution of fine modulation is correctly predicted. Figure 2(b) shows a simple schematic of the maps in Figs. 1(b) and 2(a).

To demonstrate that seeding with a chirped pulse is equivalent to quasimonochromatic stimulation with a swept source, we simulate excitation with a variable-wavelength seed pulse (2 ps duration, transform limited) at fixed delay ($\tau \sim 0$). Figure 2(c) shows the spectral output as a function of seed wavelength near the optimal seeding delay, showing results similar to a simulation from Ref. [18] with uniform envelope modulation. The diagonal seeded MI structure seen in both the simulation and the maps shown in Figs. 1(b) and 2(a) validates the interpretation in terms of scanned quasi-cw excitation. Furthermore, it explains why the experimental seeding was not exceedingly sensitive to the specific seed spectral density and peak wavelength; rather, the process was already saturated across most of the MI bandwidth by the seed pedestal. If the experimental

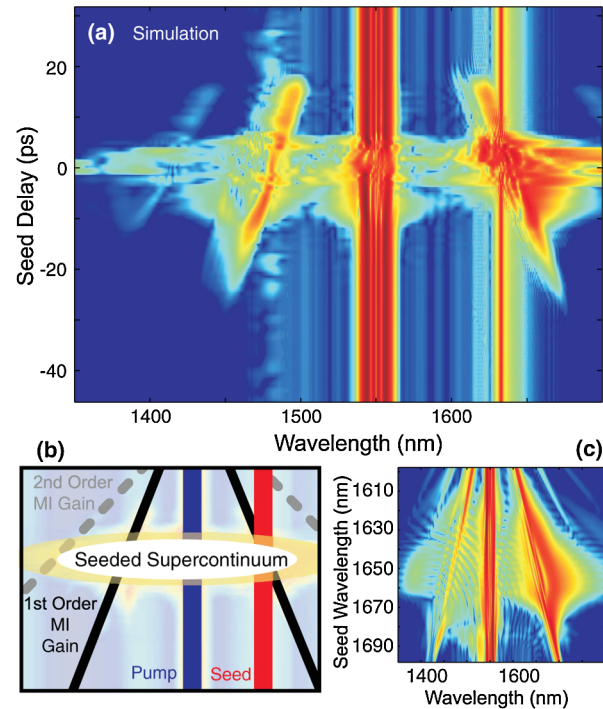


FIG. 2 (color online). (a) Simulated output spectral density [dB, color scale as in Fig. 1(b)] from the HNLF as a function of seed time delay. (b) Schematic diagram of features contained in spectral maps of Figs. 1(b) and 2(a). (c) Simulated output spectral density (color scale, dB) from the HNLF as a function of seed center wavelength (seed delay $\tau = 0$).

seed spectrum is used instead of a constant seed amplitude, the similarity between the delay and wavelength maps can be further enhanced.

We have also experimentally characterized the dependence of the seeding process on both seed and pump power levels [cf. Figs. 3(a) and 3(b), respectively]. A single soliton is ejected at a threshold pump or seed level. It can be seen that the soliton wavelength, and hence the SC bandwidth, increases *linearly* with pump power and *logarithmically* with seed power. These dependencies are consistent with the concept that MI amplifies the seed, which in turn induces soliton fission. The maximum soliton number is ultimately limited by the pump power in the presence of a strong seed; in the present regime, a substantial fraction of the pump can be transferred to a single soliton. The stable seeding process results in controlled soliton emission, whereas, noise-seeded MI leads to (pulse-to-pulse) soliton number fluctuations.

In order to demonstrate the enhanced stability afforded by seeding, we measure the noise in the RF domain as described above. Figure 3(c) shows representative RF spectra ($\lambda \sim 1685$ nm, $\Delta\lambda \sim 8$ nm) for seeded and unseeded SC with the same average redshifted power. A significant noise reduction of 30 dB is observed in the seeded scenario. It should be noted that this measurement is performed in a portion of the spectrum near the peak of the soliton, where even unseeded SC noise is minimized

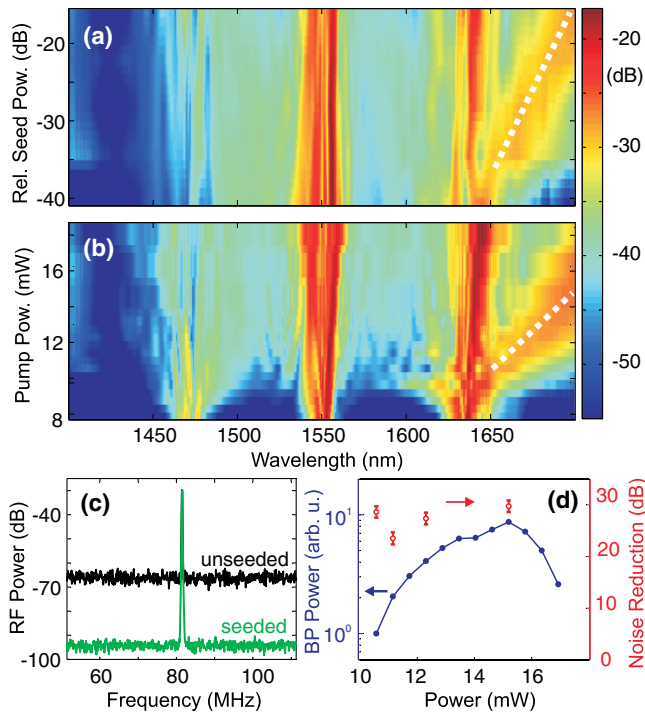


FIG. 3 (color online). Measurement of SC spectral density vs wavelength as a function of relative seed (a) and average pump power (b). Dotted lines label the soliton peak. (c) Representative experimental RF spectra for band pass-filtered seeded and unseeded supercontinua with same average redshifted power. (d) Measurement of band pass-filtered SC output power ($\lambda \sim 1685$ nm, $\Delta\lambda \sim 8$ nm) vs average pump power (left axis). Measured RF noise reduction from unseeded to seeded SC vs band pass-filtered power (right axis). Pump power adjusted for unseeded case to keep the band pass-filtered power the same.

[10]. This is likely due to the presence of a local spectral maximum where soliton timing jitter has less effect on the RF measurement. This renders the observed noise reduction obtained with seeding especially significant. With increasing pump power, the redshifted power within the measured bandwidth rises as the soliton moves into the filter window, and decreases as the soliton redshifts out of the window [cf. Figure 3(d)]. As shown, the noise reduction from the unseeded to the seeded SC remains significant throughout this range of pump power.

Evidence of stability enhancement in other spectral regions can also be indirectly inferred from the stable fine spectrotemporal structure in the experimental data (Fig. 1). In contrast, relatively featureless spectra are typically seen in ordinary long-pulse (unseeded) SC generation because the fluctuating fine structure of individual pulse spectra is lost with averaging. We also expect that the stability of the seeded SC can be further improved using an OPO optimized for operation at the necessary wavelengths and bandwidths.

In summary, using the two-color output from a parametric oscillator, we have demonstrated low-noise SC generation in the long-pulse regime, and have used this approach to investigate the properties of MI gain and

MI-induced soliton fission. The seed delay, wavelength, and both pump and seed power level dependencies of the seeding process have been characterized in this study. We have demonstrated the improvement in SC stability imparted by seeding, as evidenced by both the features in the optical spectra and the reduction in RF noise. Finally, we also note that parametric seeding can be potentially combined with the passive approaches (involving dispersion-managed fibers) mentioned in the introduction to further reduce SC noise. Generally, any form of spontaneous instability can be seeded, which will expand the relevance of the present approach to multiple applications, including ones involving different dispersion regimes and wavelengths. Parametric seeding can also be implemented with both solid-state and fiber-based sources.

This work was supported by NSF. C.R. acknowledges funding by the Deutsche Forschungsgemeinschaft (DFG-ZUK 45/1). We thank H. Fetterman for the optical source.

- [1] T. Udem, R. Holzwarth, and T.W. Hänsch, *Nature (London)* **416**, 233 (2002).
- [2] R.R. Alfano, *Sci. Am.* **295**, No. 6, 86 (2006).
- [3] S.A. Diddams, L. Hollberg, and V. Mbele, *Nature (London)* **445**, 627 (2007).
- [4] D. Wildanger, E. Rittweger, L. Kastrup, and S.W. Hell, *Opt. Express* **16**, 9614 (2008).
- [5] V. Kapoor *et al.*, *Nat. Methods* **4**, 678 (2007).
- [6] J.M. Dudley, G. Genty, and S. Coen, *Rev. Mod. Phys.* **78**, 1135 (2006).
- [7] M.N. Islam *et al.*, *J. Opt. Soc. Am. B* **6**, 1149 (1989).
- [8] H. Kubota, K.R. Tamura, and M. Nakazawa, *J. Opt. Soc. Am. B* **16**, 2223 (1999).
- [9] A.L. Gaeta, *Opt. Lett.* **27**, 924 (2002).
- [10] K.L. Corwin *et al.*, *Phys. Rev. Lett.* **90**, 113904 (2003).
- [11] D.R. Solli, C. Ropers, P. Koonath, and B. Jalali, *Nature (London)* **450**, 1054 (2007).
- [12] A. Gambetta *et al.*, *Opt. Lett.* **35**, 226 (2010).
- [13] Ö. Boyraz *et al.*, *J. Lightwave Technol.* **18**, 2167 (2000).
- [14] J.N. Kutz, C. Lyngå, and B.J. Eggleton, *Opt. Express* **13**, 3989 (2005).
- [15] P.M. Moselund, Ph.D. thesis, Technical University of Denmark, 2009.
- [16] G.P. Agrawal, *Nonlinear Fiber Optics* (Academic Press, San Diego, 2007), 4th ed..
- [17] D.R. Solli, C. Ropers, and B. Jalali, *Phys. Rev. Lett.* **101**, 233902 (2008).
- [18] J.M. Dudley, G. Genty, and B.J. Eggleton, *Opt. Express* **16**, 3644 (2008).
- [19] A. Efimov and A.J. Taylor, *Opt. Express* **16**, 5942 (2008).
- [20] G. Genty, J.M. Dudley, and B.J. Eggleton, *J. Appl. Phys.* **94**, 187 (2009).
- [21] P.M. Moselund, M.H. Frosz, C.L. Thomsen, and O. Bang, *Opt. Express* **16**, 11954 (2008).
- [22] J. Herrmann *et al.*, *Phys. Rev. Lett.* **88**, 173901 (2002).
- [23] The form of the NLSE with the well-known linear approximation for Raman scattering is sufficient to account for the experimental results.